Original Article

Check for updates

Available online at
www.heca-analitika.com/hjas

Heca Journal of Applied Sciences

Vol. 3, No. 1, 2025

Enhancing TiO_2 Photoelectrode Performance: The Role of La Doping Using the Sol-Gel Process

Mifthahul Jannah [1], Nurul Azmi [2], Andi Lala [3], Zulkarnain Jalil [4] and Mursal Mursal [4,*]

[1] Master's Program in Physics, Faculty of Mathematics and Natural Sciences, Universitas Syiah Kuala, Banda Aceh 23111, Indonesia; mifthahuljannah88@usk.ac.id (M.J.)
[2] Department of Physics Education, Faculty of Teacher Training and Education, Universitas Abulyatama, Aceh Besar 23372, Indonesia; nurul.azmi_fisika@abulyatama.ac.id (N.A.)
[3] Graduate School of Mathematics and Applied Sciences, Universitas Syiah Kuala, Banda Aceh 23111, Indonesia; andy_lala@usk.ac.id (A.L.)
[4] Department of Physics, Faculty of Mathematics and Natural Sciences, Universitas Syiah Kuala, Banda Aceh 23111, Indonesia; zjalil@usk.ac.id (Z.J.); mursal.usk@unsyiah.ac.id (M.M.)

* Correspondence: mursal.usk@unsyiah.ac.id

Article History

Received 8 January 2025
Revised 9 March 2025
Accepted 18 March 2025
Available Online 24 March 2025

Keywords:
TiO_2
La doping
Photoelectrode
Surface morphology
Crystal size
DSSC

Abstract

Due to growing interest in renewable energy technologies, dye-sensitized solar cells (DSSCs) have emerged as promising alternatives to conventional photovoltaics. This study explores the enhancement of titanium dioxide (TiO_2) photoelectrodes through doping with lanthanum (La), a rare earth element known for its ability to modify semiconductors' structural and electronic properties. La-doped TiO_2 was synthesized using the sol-gel method with La concentrations ranging from 0 to 4 mol%. The resulting films were deposited onto substrates and sintered at 600 °C for 1 hour. Characterization techniques included X-ray diffraction (XRD), scanning electron microscopy with energy-dispersive spectroscopy (SEM-EDS), UV-Vis spectrophotometry, and Fourier-transform infrared spectroscopy (FTIR). XRD confirmed the anatase phase of TiO_2 and the appearance of La_2O_3 phases with doping. The smallest crystallite size (8.20 nm) and lowest bandgap energy (3.31 eV) were achieved at 1 mol% La, compared to 3.52 eV for undoped TiO_2. SEM-EDS indicated uniform La distribution, while FTIR revealed changes in surface chemistry. These results suggest that La doping, particularly at 1 mol%, can effectively enhance the optical and structural properties of TiO_2, making it a promising candidate for improved DSSC performance.

1. Introduction

Environmental issues and the depletion of energy resources are among the most pressing challenges facing the world in the next 50 years [1]. One of the main causes is the increasing consumption of energy, which has led to a rapid decline in petroleum reserves [2]. As a result, researchers are actively seeking alternative solutions, with renewable energy technologies gaining significant attention [3]. Among various renewable energy sources, solar energy stands out due to its abundance and potential to be converted into electricity [4].

To harness solar energy efficiently, cost-effective and high-performance photovoltaic devices are essential [5]. Over the past few decades, three generations of photovoltaic technologies have been developed, with Dye-Sensitized Solar Cells (DSSCs) emerging as a promising third-generation option. First introduced in 1991, DSSCs operate based on the photovoltaic principle,

where light energy excites electrons on the cell's surface [4, 6].

A DSSC consists of several key components: a substrate, a photoelectrode, a dye, an electrolyte, and a counter electrode (commonly made of carbon) [7]. The photoelectrode plays a crucial role in converting light energy into electrical energy. Typically, oxide semiconductor materials are used for photoelectrodes due to their stability against photo corrosion and their relatively low bandgap energy, which enables efficient absorption of photons within the visible light spectrum [8].

Titanium dioxide (TiO_2) is one of the most commonly used semiconductors in DSSCs because it offers several advantages such as strong photo-oxidizing power, photocatalytic activity, affordability, and availability. However, TiO_2 also has some limitations, notably its relatively large bandgap, which leads to a higher rate of electron-hole recombination [6]. To overcome these drawbacks, doping TiO_2 with other elements has been explored. Doping can modify the base material's morphology, structure, electrical, and optical properties [6, 9].

One such dopant is lanthanum (La), which has an electron configuration of $5d^16s^2$ [10]. It typically forms a stable La^{3+} ion by losing three electrons in high-energy reactions. Due to its larger ionic radius, La^{3+} can form a secondary phase within TiO_2, potentially creating a solid solution. La doping has been shown to improve the optical response of TiO_2 and reduce its bandgap, enhancing its performance in DSSCs.

Previous research by Shakir et al. [11] demonstrated that Mg-doping in TiO_2 reduced the bandgap from 3.2 eV to 2.8 eV. Changes in Mg doping levels also affected the crystal size of TiO_2, decreasing from 53.92 nm to 49.23 nm [12]. Additionally, annealing temperature influences the bandgap; higher annealing temperatures tend to reduce it further [13]. Similarly, La doping has been shown to lower the TiO_2 bandgap from 2.98 eV to 2.75 eV [14].

In this study, we investigate the effect of lanthanum (La) doping on the structural and optical properties of TiO_2 using the sol-gel method. Specifically, we examine how varying concentrations of La influence the crystallinity, bandgap, and overall performance-related characteristics of TiO_2 for potential application in DSSCs. Although previous studies have demonstrated the benefits of La doping, a detailed understanding of how different doping levels impact TiO_2 properties remains limited. Therefore, the aim of this research is to provide a comprehensive analysis of La-doped TiO_2 to optimize its potential as a photoelectrode material in dye-sensitized solar cells.

2. Materials and Methods

2.1. Synthesis of Pure and La-Doped TiO_2

The pure and La-doped TiO_2 samples were doping using the sol-gel method. The primary materials used included Titanium (IV) isopropoxide (Sigma Aldrich, 97%), Magnesium Acetate Tetrahydrate (Sigma Aldrich, 99%), and Lanthanum (III) Acetate Hydrate (Sigma Aldrich, 98%). The solvents utilized were isopropanol, distilled water, hydrochloric acid (HCl), and ethanol.

Initially, 4 mol% of Titanium (IV) isopropoxide was mixed with isopropanol and distilled water in a volume ratio of 50:5. The mixture was stirred until it turned white, indicating the beginning of hydrolysis. Subsequently, Lanthanum (III) Acetate Hydrate was added in varying concentrations (0 mol%, 1 mol%, 2 mol%, 3 mol%, and 4 mol%), followed by adding 1 mL of HCl to catalyze the reaction. The solution was stirred for 2 hours, and the gel was allowed overnight at room temperature. The resulting gel was dried in an oven, washed twice with ethanol, and further dried at 60°C. Finally, the samples were sintered at 500°C for 5 hours to obtain the desired crystalline form.

2.2. Preparation of TiO_2 Paste and Film Deposition

The TiO_2 paste was prepared by mixing the synthesized pure and La-doped TiO_2 powder with 0.76 mL of acetic acid, 10 mL of ethanol, and two drops of Triton X-100. The mixture was stirred until a homogeneous paste was formed. The paste was then deposited onto a 2.5 × 2.5 cm conductive glass substrate using the doctor blade method. After deposition, the films were sintered at 600°C for 1 hour to enhance adhesion and crystallinity.

2.3. Structural Characterization (XRD)

X-ray diffraction (XRD) analysis was carried out using a Shimadzu D-6000 diffractometer with Cu-Kα radiation. Scanning was performed at a rate of 4°/min over a 2θ range of 5° to 80° to determine the crystal structure and phase composition. The average grain size (D) was calculated using the Scherrer equation (Equation 1) [15]:

$$D = \frac{0.9\lambda}{B\cos\theta} \quad (1)$$

where D is the average grain size in angstroms (Å), λ is the X-ray wavelength, B is the full width at half maximum (FWHM) of the diffraction peak, and θ is the Bragg angle corresponding to the peak.

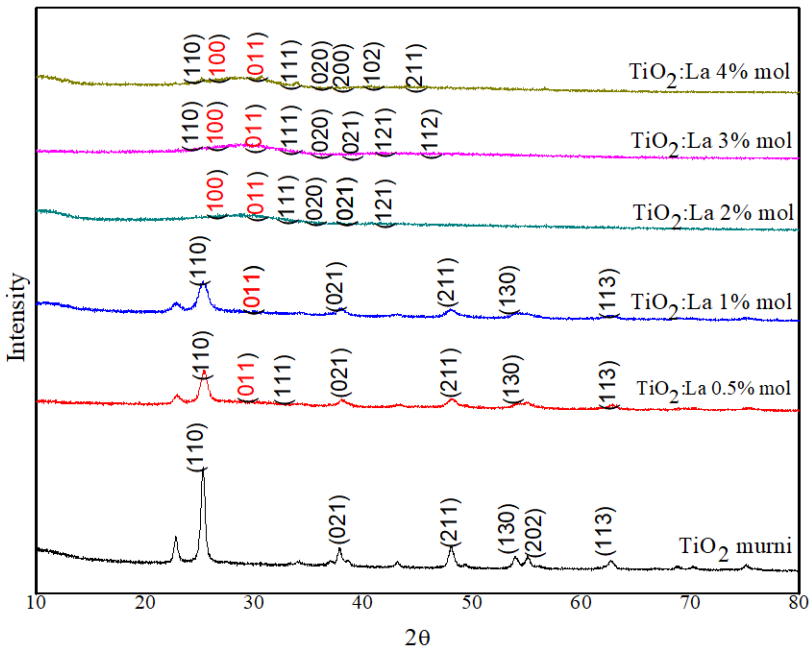

Figure 1. X-ray diffraction pattern of La-doped TiO_2 layer.

Table 1. Crystal size of TiO_2:La layers.

No	Sample Name	2θ (°)	θ (°)	FWHM	Crystal Size (nm)	Phase
1	TiO_2 (pure)	25.2580	12.6290	0.4512	19.08	TiO_2
2	TiO_2:La (0.5 mol%)	25.3574	12.6787	0.8311	10.34	TiO_2
3	TiO_2:La (1 mol%)	25.2880	12.6440	1.0475	8.20	TiO_2

2.4. Optical Property Analysis (UV-Vis)

The optical properties of the samples were analyzed using UV-Vis spectrophotometry. The photon energy (E) corresponding to the absorption wavelength was calculated using Planck's equation (Equation 2) [16]:

$$E = \frac{hc}{\lambda} \quad (2)$$

In this equation, E represents photon energy (eV), h is Planck's constant (6.626×10^{-34} J·s), c is the speed of light (3×10^8 m/s), and λ is the wavelength of the incident light (m).

2.5. Functional Group Analysis (FTIR)

FTIR spectroscopy was conducted using a Shimadzu FTIR spectrometer [17] to identify functional groups present in the samples after doping. The spectra were recorded in the 4000–400 cm^{-1} range using potassium bromide (KBr) pellets, with a wavenumber resolution of 1 cm^{-1}.

3. Results and Discussion

To identify the structure and crystal size of the TiO_2:La layers in each sample, a qualitative analysis was conducted using X-ray diffraction (XRD) with a Shimadzu instrument, employing CuKα radiation (λ = 1.54060 Å). The applied voltage was 40 kV, with a current of 30 mA. The scanning method was performed in a step mode with a data interval of 0.02°, and the detected diffraction angle (θ) ranged from 10° to 80°. Based on the XRD images and data, phase identification was done by analyzing the 2θ angles, lattice spacing (d), intensity (I/I_0), phase composition, and crystal structure. The identification process matched the obtained data with the PDF-ICDD database, using the 2θ angle as the primary reference.

Figure 1 shows the XRD spectrum of the TiO_2:La layers, revealing the presence of TiO_2 phases at 2θ = 25.26°, 48.02°, and 42.6°, while La_2O_3 phases appeared at 2θ = 25.8° and 30.56°. The most dominant diffraction peaks in the La-doped TiO_2 layers corresponded to TiO_2 in pure TiO_2 and in 0.5 mol% and 1 mol% La-doped TiO_2 samples, indicating the formation of a crystalline structure. However, the diffraction peaks showed a decrease in crystallinity for TiO_2:La samples with 2 mol%, 3 mol%, and 4 mol% doping. These predominant diffraction peaks in these samples corresponded to La_2O_3, suggesting that as the La content increased, the crystallinity of the semiconductor material was altered.

Table 1 shows the crystal size of the TiO_2:La layers. The calculations indicate that La doping reduces the crystal size of TiO_2. The largest crystal size was observed in the pure TiO_2 sample, measuring 19.08 nm. This is attributed to the small Full Width at Half Maximum (FWHM) value

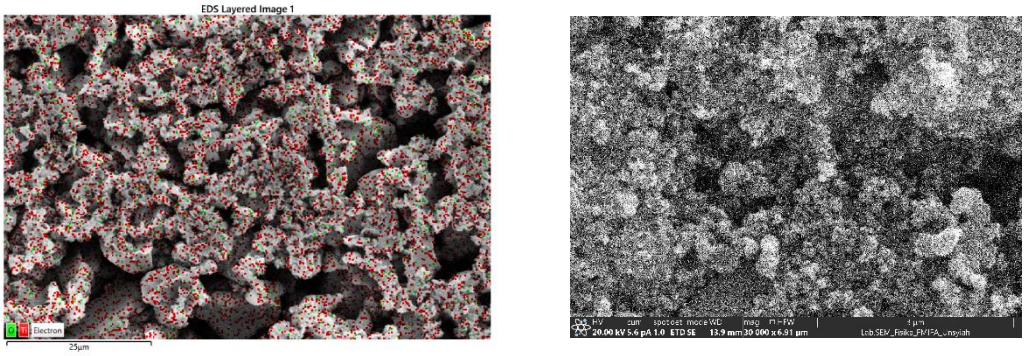

(a) **(b)**

Figure 2. The SEM images of the TiO_2:La layers: (a) pure TiO_2 and (b) TiO_2:La with 1 mol% doping.

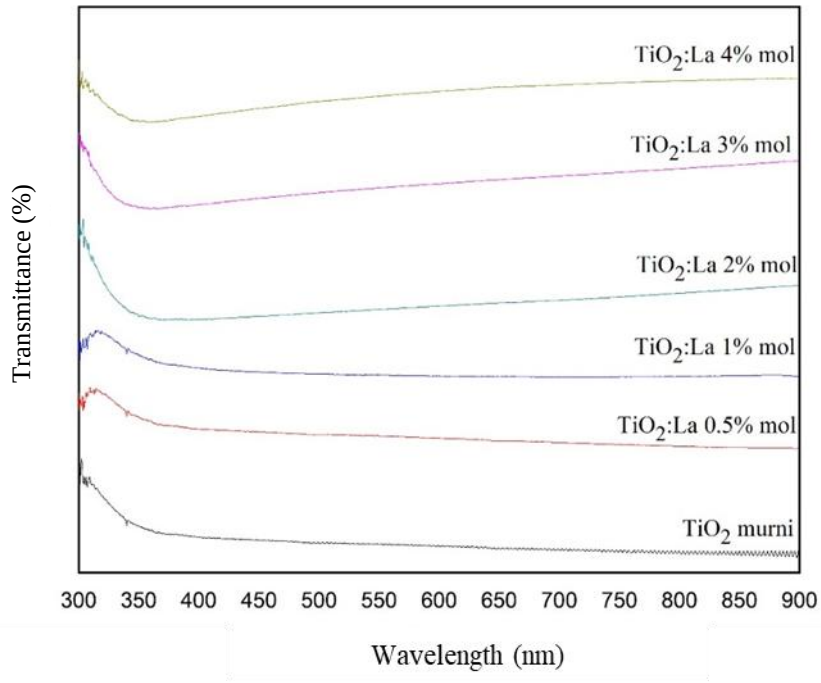

Figure 3. The transmittance graph of the La-doped TiO_2 layers.

and the narrow diffraction peaks. However, after adding 0.5 mol% and 1 mol% La doping, the TiO_2 crystal size decreased to 10.34 nm and 8.20 nm, respectively.

The results clearly show that La doping significantly affects the crystal size of TiO_2. However, at higher La doping concentrations (2 mol%, 3 mol%, and 4 mol%), the degree of crystallinity decreased, affecting the FWHM values. For these concentrations, the highest intensity diffraction peaks resulted in an FWHM value of zero, meaning the crystal size calculations had to be based on very low-intensity peaks. The zero FWHM value suggests that the structure of the material became amorphous, which was influenced by the increasing La concentration.

Figure 2 presents SEM images showing the surface morphology of TiO_2 layers: (a) pure TiO_2 and (b) TiO_2 doped with 1 mol% La. In Figure 2a, the pure TiO_2 exhibits a rough and porous structure with densely packed particles. The overlaid EDS mapping (red dots) indicates elemental distribution, suggesting a uniform composition. In contrast, Figure 2b, representing La-doped TiO_2, shows a more refined and compact surface morphology, with slightly smaller and more uniformly distributed particles. This suggests that La doping influences the growth and distribution of TiO_2 grains, contributing to the formation of a more homogeneous surface, which is beneficial for photoelectrode applications in DSSCs.

The transmittance spectrum of the La-doped TiO_2 layers is presented in Figure 3. The obtained transmittance curves indicate optical absorption in the wavelength range of 330–450 nm for all samples, including pure TiO_2 and TiO_2 doped with 0.5 mol%, 1 mol%, 2 mol%, 3 mol%, and 4 mol% La. The peak transmittance of pure TiO_2 occurred at 352 nm. After doping with 1 mol% La, the transmittance peak shifted to 374 nm, indicating increased absorption towards longer wavelengths (redshift). However, for 4 mol% La-doped TiO_2, the transmittance peak shifted back to 349.5 nm, suggesting

Table 2. Bandgap energy of TiO_2:La layers.

Sample	Cutoff Wavelength (λ_o) (nm)	Bandgap Energy (eV)
TiO_2 (pure)	352	3.52
TiO_2:La (0.5 mol%)	369	3.36
TiO_2:La (1 mol%)	374	3.31
TiO_2:La (2 mol%)	360.5	3.44
TiO_2:La (3 mol%)	347	3.57
TiO_2:La (4 mol%)	349.5	3.55

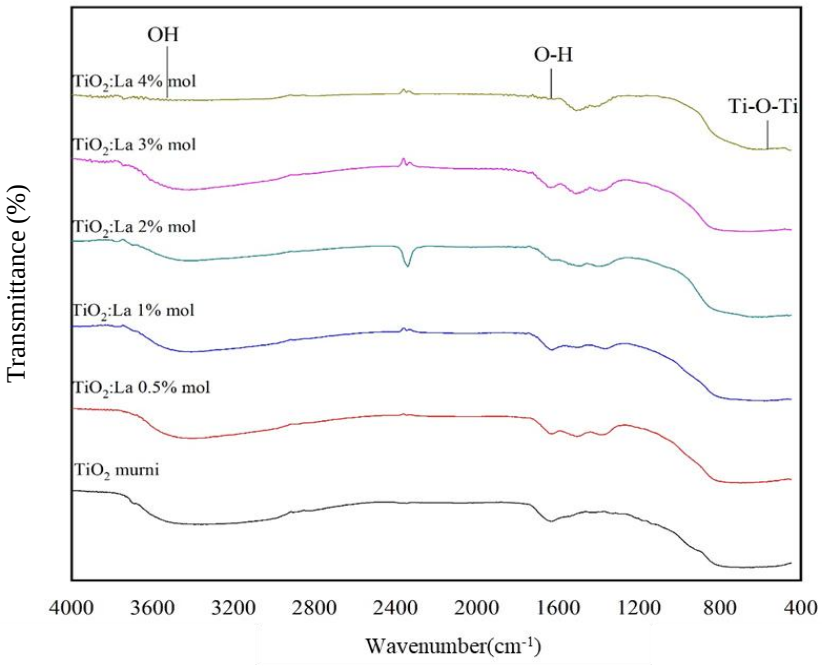

Figure 4. The FTIR spectrum of La-doped TiO_2 layers.

that excessive La doping reduces transmittance. These results indicate that as the La concentration increases, the transmittance value tends to decrease, shifting the absorption edge and influencing the optical properties of TiO_2. This suggests that La doping can effectively tune the optical behavior of TiO_2, which is beneficial for applications such as DSSCs.

As a photocatalyst, which is a material that accelerates light-induced reactions, TiO2 has a semiconductor structure with an electronic structure characterized by a filled valence band and an empty conduction band. The two bands are separated by a band gap energy of 3.2 eV for the anatase phase and 3.0 eV for the rutile phase. TiO_2 in the anatase phase has a higher activity compared to the rutile phase, In the anatase phase, TiO2 has a larger surface area and smaller size compared to rutile.

Table 2 shows that variations in La doping concentration significantly affect the bandgap energy of TiO_2. The bandgap of pure TiO_2 was measured at 3.52 eV. After doping with 1 mol% La, the bandgap decreased to 3.31 eV, indicating improved light absorption and potential enhancement in DSSC performance. The bandgap reduction in La-doped TiO_2 is more pronounced than Mg-doped TiO_2, as La has a lower intrinsic bandgap than Mg. However, at higher La doping concentrations (3 mol% and 4 mol%), the bandgap increased to 3.57 eV and 3.55 eV, respectively. This increase is due to the excessive La content, which disrupts the TiO_2 crystal structure and reduces its crystallinity.

Reducing the bandgap through doping can minimize premature electron recombination during the excitation process, making La-doped TiO_2 a promising material for use as a photoelectrode in DSSCs. However, excessive La doping may negatively impact the material's electronic properties.

Figure 4 presents the FTIR spectrum of La-doped TiO_2 layers. The spectrum reveals the Ti-O-Ti polymer chain at 530 cm^{-1}, indicating the presence of TiO_2 bonding structures. The O-H vibrational mode is observed at 3414 cm^{-1} and 1635 cm^{-1}, suggesting hydroxyl (-OH) group vibrations commonly associated with surface moisture or absorbed water. Incorporating La^{3+} ions into the TiO_2 matrix influences the adsorption of H_2O molecules on the material's surface. Despite testing six different La doping concentrations, the FTIR spectra showed no significant differences in peak positions. However, the addition of La

affected the H_2O-related functional groups, indicating that La doping alters the surface chemistry of TiO_2 (Huang et al., 2017). This surface modification could potentially enhance the photocatalytic activity and DSSC performance of La-doped TiO_2 by improving dye adsorption and charge transport.

Based on the crystal structure analysis, adding La doping alters the crystal structure of TiO_2 and reduces its grain size. A smaller grain size enhances the dye adsorption capability of the La-doped TiO_2 layer, which is beneficial for DSSC applications. From an optical perspective, La doping also reduces the energy gap of TiO_2. A lower bandgap facilitates electron excitation from the valence band to the conduction band, allowing more sunlight absorption by the La-doped TiO_2 layer. The experimental results indicate that La-doped TiO_2 has significant potential as a photoelectrode material for DSSCs, as it improves both optical and structural properties, leading to enhanced solar energy conversion efficiency. This includes categorizing the DSSC manufacturing process and comparing it to solar cell applications [18].

4. Conclusions

Based on the results of this study, it can be concluded that La doping enhances the crystallinity of TiO_2 compared to the undoped sample. The smallest crystallite size, 8.20 nm, was observed at a La concentration of 1 mol%. Surface morphology analysis showed a homogeneous distribution, and SEM-EDS results indicated that the atomic percentage of Ti decreased with increasing La concentration, suggesting successful substitution of Ti by La in the TiO_2 lattice. The lowest energy bandgap, 3.31 eV, was also achieved at 1 mol% La doping, confirming that La incorporation effectively reduces the bandgap of TiO_2. FTIR analysis revealed characteristic Ti–O–Ti and Ti–O bonds at 530 cm^{-1} and 789 cm^{-1}, respectively, along with increased H_2O absorption in La-doped samples. TiO_2 doped with 1 mol% La shows the most favorable structural and optical properties, indicating its strong potential as a photoelectrode material for DSSC applications.

Author Contributions: Conceptualization, Z.J. and M.M.; methodology, M.J. and A.L.; software, M.J.; validation, M.J., N.A., and A.L.; formal analysis, M.J.; investigation, M.J.; resources, A.L.; data curation, M.J.; writing—original draft preparation, M.J.; writing—review and editing, A.L. and M.M.; visualization, M.J.; supervision, Z.J. and M.M.; project administration, M.M.; funding acquisition, M.M. All authors have read and agreed to the published version of the manuscript.

Funding: This study does not receive external funding.

Ethical Clearance: Not applicable.

Informed Consent Statement: Not applicable.

Data Availability Statement: The data is available to the corresponding author upon request.

Conflicts of Interest: All the authors declare no conflicts of interest.

References

1. Pang, L., Liu, L., Zhou, X., Hafeez, M., Ullah, S., and Sohail, M. T. (2024). How Does Natural Resource Depletion Affect Energy Security Risk? New Insights from Major Energy-Consuming Countries, *Energy Strategy Reviews*, Vol. 54, 101460. doi:10.1016/j.esr.2024.101460.

2. Hilmi, E., Yandri, E., Uhanto, U., Saiful, R., and Hamja, N. (2024). Hybrid Energy Solutions for Sustainable Offshore Oil and Gas Operations: Leveraging Thermoelectric, Solar, and Wind Potential, *Leuser Journal of Environmental Studies*, Vol. 2, No. 2, 52–61. doi:10.60084/ljes.v2i2.218.

3. Aprianto, A., Maulana, A., Noviandy, T. R., Lala, A., Yusuf, M., Marwan, M., Afidh, R. P. F., Irvanizam, I., Nizamuddin, N., and Idroes, G. M. (2023). Exploring Geothermal Manifestations in Ie Jue , Indonesia : Enhancing Safety with Unmanned Aerial Vehicle, *Leuser Journal of Environmental Studies*, Vol. 1, No. 2, 47–54. doi:10.60084/ljes.v1i2.75.

4. Ako, R. T., Ekanayake, P., Tan, A. L., and Young, D. J. (2016). La Modified TiO2 Photoanode and Its Effect on DSSC Performance: A Comparative Study of Doping and Surface Treatment on Deep and Surface Charge Trapping, *Materials Chemistry and Physics*, Vol. 172, 105–112. doi:10.1016/j.matchemphys.2015.12.066.

5. Wang, Y., and Zuo, L. (2024). High-Performance and Multifunctional Organic Photovoltaic Devices, *Journal of Zhejiang University-SCIENCE A*, Vol. 25, No. 10, 841–853. doi:10.1631/jzus.A2400015.

6. Dette, C., Pérez-Osorio, M. A., Kley, C. S., Punke, P., Patrick, C. E., Jacobson, P., Giustino, F., Jung, S. J., and Kern, K. (2014). TiO 2 Anatase with a Bandgap in the Visible Region, *Nano Letters*, Vol. 14, No. 11, 6533–6538. doi:10.1021/nl503131s.

7. Karim, N. A., Mehmood, U., Zahid, H. F., and Asif, T. (2019). Nanostructured Photoanode and Counter Electrode Materials for Efficient Dye-Sensitized Solar Cells (DSSCs), *Solar Energy*, Vol. 185, 165–188. doi:10.1016/j.solener.2019.04.057.

8. Xia, C., Wang, H., Kim, J. K., and Wang, J. (2021). Rational Design of Metal Oxide-Based Heterostructure for Efficient Photocatalytic and Photoelectrochemical Systems, *Advanced Functional Materials*, Vol. 31, No. 12. doi:10.1002/adfm.202008247.

9. Jiang, Y., Zheng, B., Du, J., Liu, G., Guo, Y., and Xiao, D. (2013). Electrophoresis Deposition of Ag Nanoparticles on TiO2 Nanotube Arrays Electrode for Hydrogen Peroxide Sensing, *Talanta*, Vol. 112, 129–135. doi:10.1016/j.talanta.2013.03.015.

10. Manikandan, A., Manikandan, E., Meenatchi, B., Vadivel, S., Jaganathan, S. K., Ladchumananandasivam, R., Henini, M., Maaza, M., and Aanand, J. S. (2017). Rare Earth Element (REE) Lanthanum Doped Zinc Oxide (La: ZnO) Nanomaterials: Synthesis Structural Optical and Antibacterial Studies, *Journal of Alloys and Compounds*, Vol. 723, 1155–1161. doi:10.1016/j.jallcom.2017.06.336.

11. Shakir, S., Abd-ur-Rehman, H. M., Yunus, K., Iwamoto, M., and Periasamy, V. (2018). Fabrication of Un-Doped and Magnesium Doped TiO2 Films by Aerosol Assisted Chemical Vapor Deposition for Dye Sensitized Solar Cells, *Journal of Alloys and Compounds*, Vol. 737, 740–747. doi:10.1016/j.jallcom.2017.12.165.

12. Khan, F. U., Zubair, M., Ansar, M. Z., Alamgir, M. K., and Nadeem, S. (2016). Effect of Annealing Temperature on the Structural and Optical Properties of TiO2 Thin Film Prepared by Sol-gel Method, *Journal of Scientific Research*, Vol. 8, No. 3, 267–272. doi:10.3329/jsr.v8i3.27195.

13. Xu, L., Li, X., Chen, Y., and Xu, F. (2011). Structural and Optical Properties of ZnO Thin Films Prepared by Sol–Gel Method with Different Thickness, *Applied Surface Science*, Vol. 257, No. 9, 4031–4037. doi:10.1016/j.apsusc.2010.11.170.

14. Huang, Y., Ho, S. S. H., Ho, K. F., Lee, S. C., Yu, J. Z., and Louie, P. K. K. (2011). Characteristics and Health Impacts of VOCs and Carbonyls Associated with Residential Cooking Activities in Hong Kong, *Journal of Hazardous Materials*, Vol. 186, No. 1, 344–351. doi:10.1016/j.jhazmat.2010.11.003.

15. Ulhakim, M. T., Sukarman, S., Khoirudin, K., Fazrin, N., Irfani, T., and Hakim, A. (2024). Determining The Crystallite Size of TiO2/EG-Water XRD Data Using the Scherrer Equation, *Indonesian Journal of Applied Physics*, Vol. 14, No. 1, 141. doi:10.13057/ijap.v14i1.79195.

16. Bachvarova-Nedelcheva, A., Iordanova, R., Georgieva, N., Nemska, V., Foteva, T., and Stoyanova, A. (2024). Influence of Nb2O5 and B2O3 on the Photocatalytic and Antibacterial Activity of Sol-Gel Derived TiO2 Nanopowders, *Journal of Chemical Technology and Metallurgy*, Vol. 59, No. 2, 335–342.

17. Sufriadi, E., Meilina, H., Munawar, A. A., and Idroes, R. (2021). Fourier Transformed Infrared (FTIR) Spectroscopy Analysis of Patchouli Essential Oils Based on Different Geographical Area in Aceh, *IOP Conference Series: Materials Science and Engineering*, Vol. 1087, No. 1, 012067. doi:10.1088/1757-899X/1087/1/012067.

18. Gohar, O., Zubair Khan, M., Bibi, I., Bashir, N., Tariq, U., Bakhtiar, M., Ramzan Abdul Karim, M., Ali, F., Bilal Hanif, M., and Motola, M. (2024). Nanomaterials for Advanced Energy Applications: Recent Advancements and Future Trends, *Materials & Design*, Vol. 241, 112930. doi:10.1016/j.matdes.2024.112930.